Vol 15 No 4, April 2006
1009-1963/2006/15(04)/0767-06

Chinese Physics

© 2006 Chin. Phys. Soc.
and IOP Publishing Ltd

Enhancing low-field magnetoresistance of $La_{0.67}Ca_{0.33}MnO_3$ films deposited on anodized aluminium-oxide membranes*

Tang Wei-Hua(唐为华)[a)b)†], Li Pei-Gang(李培刚)[b)], Lei Ming(雷 鸣)[b)], Guo Yan-Feng(郭艳峰)[b)], Chen Lei-Ming(陈雷明)[b)], Li Ling-Hong(李玲红)[c)], Song Peng-Yun(宋朋云)[d)], and Chen Chinping(陈晋平)[d)]

[a)] *Department of Physics, Centre for Optoelectronics Materials and Devices, Zhejiang Sci-Tech University, Xiasha College Park, Hangzhou* 310018, *China*

[b)] *Beijing National Laboratory for Condensed Matter Physics, and Institute of Physics, Chinese Academy of Sciences, Beijing* 100080, *China*

[c)] *Department of Physics, University of Dayton, Dayton, OH*45469, *USA*

[d)] *Department of Physics, Peking University, Beijing* 100871, *China*

(Received 30 September 2005; revised manuscript received 23 February 2006)

In this paper we report a new method to fabricate nanostructured films. $La_{0.67}Ca_{0.33}MnO_3$ (LCMO) nanostructured films have been fabricated by using pulsed electron beam deposition (PED) on anodized aluminium oxide (AAO) membranes. The magnetic and electronic transport properties are investigated by using the Quantum Design physics properties measurement system (PPMS) and magnetic properties measurement system (MPMS). The resistance peak temperature (T_p) is about 85 K and the Curie temperature (T_c) is about 250 K for the LCMO film on an AAO membrane with a pore diameter of 20 nm. Large magnetoresistance ratio (MR) is observed near T_p. The MR is as high as 85 % under 1 T magnetic field. The great enhancement of MR at low magnetic fields could be attributed to the lattice distortion and the grain boundary that are induced by the nanopores on the AAO membrane.

Keywords: colossal magnetoresistance, nanostructured film, transport properties
PACC: 5225F, 7000, 7130, 7570P

1. Introduction

Colossal magnetoresistance (CMR) in rare earth perovskite manganites has attracted attention because of their potential applications in magnetoresistive transducers and sensors. High MR ratio under low magnetic fields is very important in sensor applications. CMR effects in bulk forms or thin films have been extensively studied,[1–3] but high MR ratio at low magnetic fields is hard to obtain. The electrical and magnetic properties of manganese perovskites strongly depend on strain, grain size and grain boundary. Grain size reduction results in increasing resistivity and decreasing metal-insulator transition temperature.[4] In recent years, nanostructured materials have attracted much attention due to their unusual properties.[5–8] For La–Ca–Mn–O (LCMO) nano-crystalline grain with an average particle size of 30 nm, its ferromagnetic transition temperature is 300 K, which is about 50 K higher than that of its single crystal.[9] The magnetoresistance increases with grain size decreasing at low temperatures.[10] All of these results indicate that the manganese perovskites on a nanoscale could be quite different in comparison with those in the bulk forms. Thus, we believe that studies of the manganese perovskites under nanometre scale may offer great opportunities to explore the intriguing physics and the potentials for device applications. Gong *et al* obtained nano-dots on the surface of $La_{0.5}Ca_{0.5}MnO_3$ thin film by annealing the film at a high temperature, and found the

*Project supported by the key program of Natural Science Foundation of Zhejiang Provincial, China (Grant No Z605131), National Natural Science Foundation of China (Grant No 60571029), the 'Hundred Talents Project' of Chinese Academy of Sciences, China, the Creative Research Group of the National Natural Science Foundation of China (Grant No 60321001).

†E-mail: whtang@zist.edu.cn

magnetoresistance to be enhanced.[11] As an important preparation method, the template method has been successfully used for the synthesis of nanostructured materials.[12−14] The two-dimensional Fe nanostructured network has been deposited by dc sputtering on the nanochannel alumina. The Fe nanostructured network shows its coercivity to be dramatically enhanced compared with the continuous Fe film with the same thickness,[15] and the antiferromagnetic/ferromagnetic coupled nanostructured bilayers exhibit their exchange bias and coercivity to be augmented.[16] Zhao *et al* reported nanostructured LCMO prepared by pulsed-laser-deposition on the surface of porous Al_2O_3.[17] In this work, we prepare $La_{0.67}Ca_{0.33}MnO_3$ films on anodized aluminium oxide (AAO) membranes by using pulsed electron beam deposition (PED), and the enhanced MR ratio is obtained under a low magnetic field.

2. Experimental

Nanostructured LCMO thin films were deposited by using the pulsed electron deposition technique. The anodized aluminium oxide (AAO) membranes were used as substrates for the growing of LCMO thin films. AAO membranes were fabricated by using a two-step anodization process.[18] The substrate temperature was around 973 K, and the deposition atmosphere was pure oxygen at a pressure of 1.5Pa. After the deposition, the LCMO thin films were annealed at 1023 K for 30 minutes in an oxygen atmosphere at a pressure of 101Pa. The LCMO thin films grown on the $SrTiO_3$ (100) substrate under the same deposition condition were used to calibrate the film thickness on the AAO membranes. Dektak 8 surface profiler was used to measure the film thickness. The morphology of LCMO thin films on AAO membranes was studied by using DB235 focused ion beam system. The magnetic and electronic transport properties of LCMO thin films were measured using PPMS and MPMS systems.

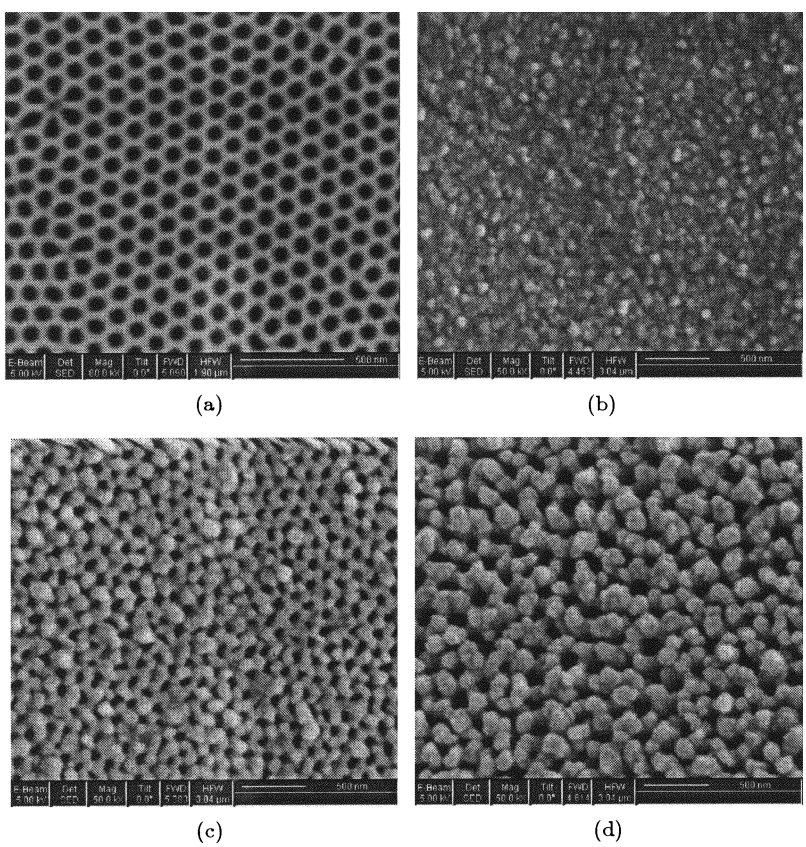


Fig.1. The SEM images of AAO membrane (a) and morphologies of LCMO films on AAO membranes with pore diameters of 20 nm (b), 70 nm (c) and 100 nm (d).

3. Results and discussion

Figure 1 shows the SEM images of AAO membrane (a) and the morphologies of LCMO films on AAO membranes with different pore diameters (b)–(d). It can be seen that LCMO is deposited along the wall of the pore, forming an ordered hexagonal LCMO networks on AAO with larger pore diameters (70 nm and 100 nm). The LCMO film on AAO with a smaller pore diameter (20 nm) shows the feature of grained film. The morphology of LCMO film changes with the reduction of pore diameter, which provides a way to control the morphology of the film by adjusting the pore diameter. The result of Detak8 shows that the thickness of LCMO film is about 100 nm.

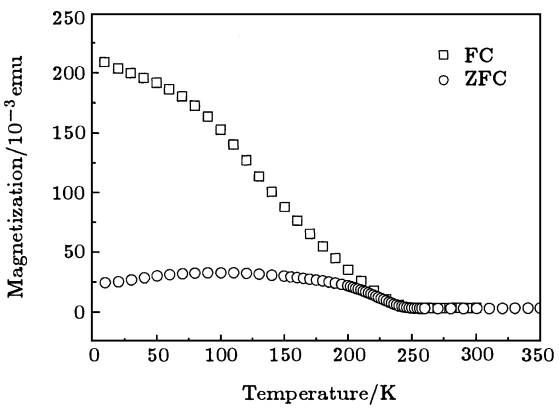


Fig.2. Temperature-dependent of the magnetizations of ZFC and FC for the LCMO film on the AAO membrane with a pore diameter of 20 nm.

The temperature-dependent magnetizations with zero field cooling (ZFC) and field cooling (FC) were measured using the MPMS system. The ZFC magnetization was measured in the warming process with a magnetic field of 0.01 T applied after cooling the sample down to 5 K without magnetic field, and the FC magnetization was measured in the warming process with a magnetic field of 0.01 T applied after cooling the sample down to 5 K under 1 T magnetic field. The results are shown in Fig.2. The Curie temperature (T_c) is about 250 K. The transition from paramagnetism to ferromagnetism takes place in a very broad temperature range. The ZFC and FC curves are split below the paramagnetic–ferromagnetic transition. This could result from the size effect of LCMO, as reported in Ref.[10], and high degree of disordered spin orientation at the interface of grain boundary. When the sample cools under a magnetic field, part of disordered spins are oriented, thus the magnetization at lower temperatures is larger than that at higher temperatures. When the sample cools under no magnetic field, those spins will keep disordered and frozen at low temperatures, thus the magnetization of ZFC is lower than that of FC.

To check our measuring system, the I-V curves at different temperatures were measured first and the results are shown in Fig.3. The linear I-V curves indicate that during measuring the electrical probes are in ohmic contact with the film and there exist no electronic tunnelling effect in the film in the whole temperature range. Figure 4 shows the temperature-dependent resistances under different magnetic fields. To avoid the thermal hysteresis effect, data were taken in the cooling process, as shown in Fig.4. It is found that in the absence of magnetic field T_p is about 85 K, much lower than that of a usual bulk material or thin film. The T_p shifts to higher temperatures and the resistance below T_p is suppressed significantly when the magnetic field is increased. The magnetoresistance ratio, which is defined as MR=$[R(0)–R(H)]/R(0)$, versus temperature under different magnetic field are shown in Fig.5. The MR ratio is as high as 85 % under 1 T at 75 K. Such a large MR at low magnetic fields has not been reported for bulk or thin film samples before. The high field MR reaches nearly 100% and the MR remains almost unchanged at low temperatures.

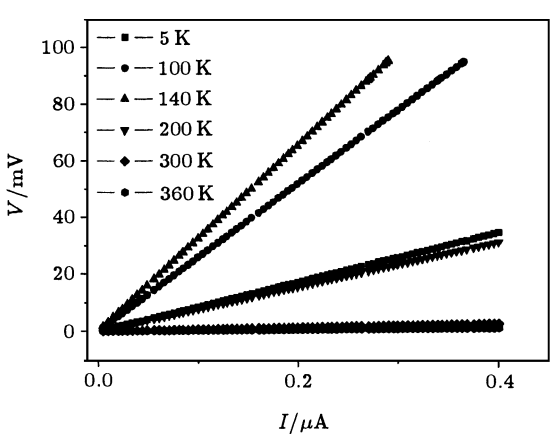


Fig.3. I-V curves at different temperatures for the LCMO film on the AAO membrane with a pore diameter of 20 nm.

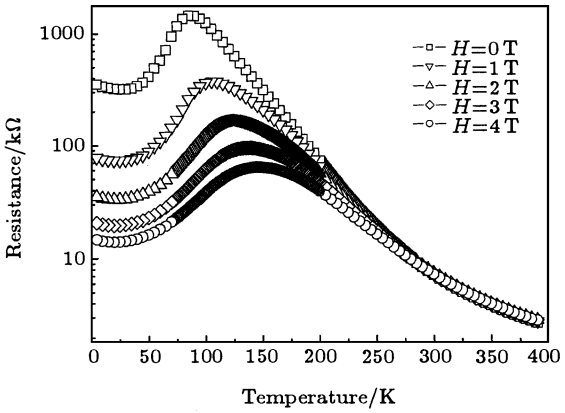


Fig.4. Temperature-dependent resistances under different magnetic fields.

It is considered that there are two possible causes that can result in the large low-field magnetoresistance: one is lattice distortion and the other is grain boundary. Alumina crystallizes in a tetragonal structure with a lattice parameters of a=4.76Å, c=12.99Å, and LCMO is a pseudo cubic structure with a lattice parameter of a=3.87Å, thus large mismatch stress exists between LCMO and AAO. A larger substrate-induced lattice distortion leads to a larger zero-field resistivity and larger negative magnetoresistance. The substrate-induced lattice distortion includes lattice strain and lattice relaxation. The lattice strain yields intrinsic effects on the phonon modes and magnetic exchange interaction; the lattice relaxation yields extrinsic effects such as dislocations and domain walls. The incompletely aligned moments of the magnetic domains due to either inhomogeneity or pinning by local defects below T_c give rise to larger scattering of conduction electrons. Therefore when a magnetic field is applied the magnetic domains are aligned, thereby the resistivity will decrease largely in samples with the larger lattice distortion being formed.

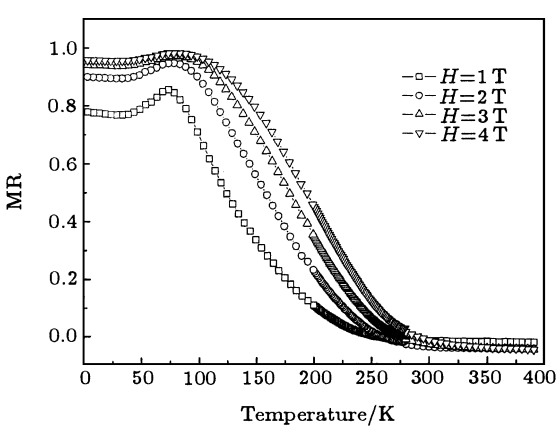


Fig.5. Magnetoresistance versus temperature under different magnetic fields.

Besides the effect of the lattice disorder between the film and substrate, the grain size and grain boundaries could play a more important role in achieving a large MR under low-fields. The LCMO film on AAO with a pore diameter of 20 nm shows the feature of grained film. For the magnetic matrix, the grain size and grain boundaries play important roles in the spin-dependent tunnelling and scattering of the conducting electrons. The spins on the interfaces of magnetic particles are disordered because of the coexistence of broken bonds and symmetry breaking, and the magnetic coupling of the interfacial spins is weaker than that of spins in the grain. The structural disorder on the interfaces induces the interfacial disordered spin state or spin glass state. As a result the magnetic particles form a core-shell structure[19] in which the core is metal-ferromagnetic and the shell is insulated and spin is disordered. The shells are the barriers for the conducting electrons, and increase the resistance of the film. When a magnetic field is applied, the disordered spins on the interfaces are directed towards the field direction, and the resistance will decrease. This is maybe another cause for low-field magnetoresistance.

The following three models are usually used to describe above T_c for CMR samples. In the small polaron hopping (SPH) model, the temperature-dependent resistivity is expressed as

$$\rho = AT\exp(E_a/k_BT) \tag{1}$$

where A is a constant, k_B is the Boltzmann constant and E_a is the activation energy.

In the variable range hopping (VRH) model, the temperature-dependent resistivity is given by

$$\rho = A\exp(T_0/T)^{1/4} \tag{2}$$

with

$$T_0 = 1.5/\xi^3 k_B N(\varepsilon_F) \tag{3}$$

where ξ is the hopping constant, $N(\varepsilon_F)$ is the state density of Fermi surface.

In the semiconductor (SEM) model, the temperature-dependent resistivity is written as

$$\rho = A\exp(E_g/k_BT) \tag{4}$$

where A is a constant and E_g is the energy gap.

We fit the data with these models, the relevant parameters are given in Table 1. Though these models are for temperature-dependent resistivity, the curve is for temperature-dependent resistance in Fig.6. The fitting curves are plotted in Fig.6. It is seen that the SPH model fits our experimental data best.

Table 1. The fitting parameters with different models.

Model	Formula	Fitting Parameters
SPH	$\rho = AT\exp(E_a/k_BT)$	A=4.1×10^{-4}, E_a=0.12eV
VRH	$\rho = A\exp(T_0/T)^{1/4}$	A=2.1×10^{-7}, T_0 =2.9×10^7
SEM	$\rho = A\exp(E_g/k_BT)$	A=0.24, E_g =0.09eV

At low temperatures, we fit the resistance with the law

$$R = R_0 + AT^a + BT^b \qquad (5)$$

where a=1.5 or 2, b=4.5 or 5. $T^{1.5}$ is attributed to the effect of electron scattering in spin glass, T^2 to the effect of electron–electron scattering, $T^{4.5}$ to the effect of electron–magnon scattering, and T^5 to the effect of electron-phonon scattering. Using Eq.(5) to fit the experimental data, a=2 and b=5 are found to be more suitable. The following values are used: R_0=337.36, A=4.48×10^{-7} and B=0.027. Thus electron–electron scattering and electron–phonon scattering are the main mechanism at low temperatures.

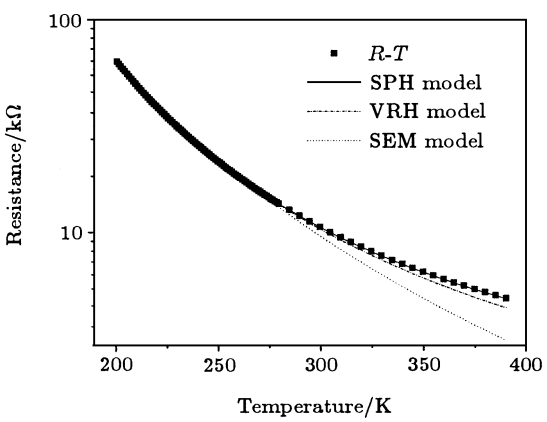


Fig.6. Temperature-dependent resistances above T_c fitted with three models.

The low temperature transport properties appear to be strongly correlated with the grain boundaries and magnetic domain wall scattering as well. The upturn of resistance curve at low temperatures as shown in Fig.7, is maybe because of weak localization, which the $T^{1/2}$ regime is ascribed to it. The inset of Fig.7 shows our fitting result. A characteristic signature of weak localization is the strong temperature-dependent negative magnetoresistance at low temperatures.

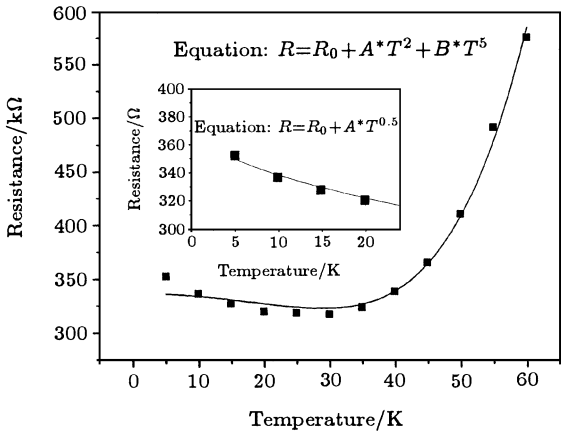


Fig.7. Temperature-dependent resistance in the metallic regime fitted with Eq. 5 shown as solid line, the inset is for fitting with $AT^{1/2}$ at low temperatures.

Figure 8 shows the cooling resistance and warming resistance under zero-field. It can be seen that there exists a significant difference between two curves. The cooling resistance is much higher than the warming resistance and reaches a maximum value near T_p. The strong temperature-hysteresis observed at the metal-insulator transition indicates that this is a strong first-order transition. We call it hysteretic resistance (HR), which is defined as

$$\mathrm{HR} = (R(H)_c - R(H)_w)/R(H)_c, \qquad (6)$$

where $R(H)_c$ and $R(H)_w$ are the cooling resistance and the warming resistance with magnetic field H respectively. Figure 9 indicates the HR varying with temperature under different magnetic fields. With the increase of applied magnetic field, the HR reduces and its peak shifts to higher temperatures.

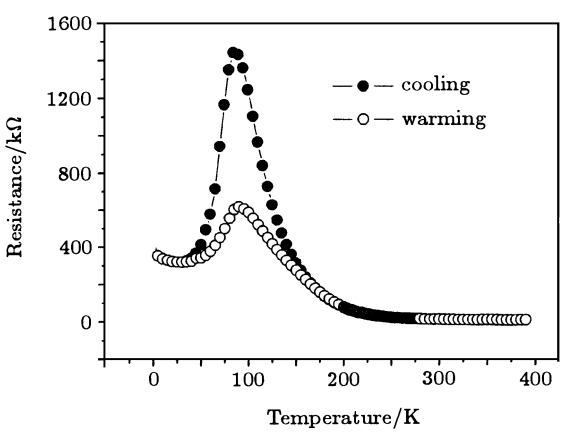


Fig.8. Temperature-dependent resistance during cooling and warming respectively.

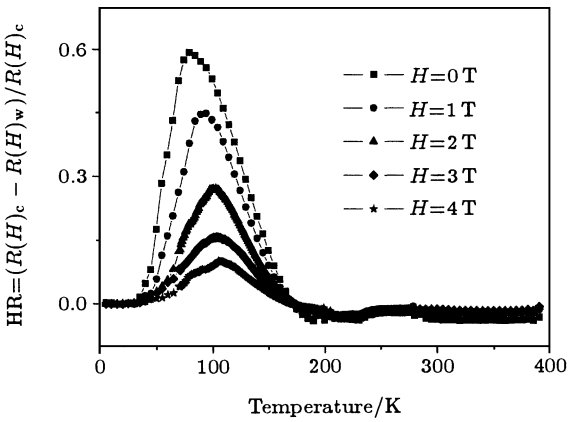


Fig.9. Temperature-dependent HR under different magnetic fields.

4. Conclusions

The transport properties and magnetic properties of an LCMO film on the AAO membrane with a pore diameter of 20 nm are investigated. The resistance peak temperature (T_p) is about 85 K, and the Curie temperature (T_c) is about 250 K. 85 % magnetoresistance is found for the film under a 1 T magnetic field. The considerable enhancement MR at low magnetic fields could be attributed to the lattice distortion and the grain boundary that are induced by the nanopores on the AAO membrane.

References

[1] Canedy C L, Ibsen K B, Xiao G, Sun J Z, Gupta A and Gallagher W J J 1996 *Appl. Phys.* **79** 4546
[2] Rivas J, Hueso L E, Fondado A, Rivadulla F and Quintela M A L 2000 *J. Magn. Magn. Mater.* **221** 57
[3] Mccormack M, Jin S, Tiefel T H, Fleming R M, Phillips J M and Ramesh R 1994 *Appl. Phys. Lett.* **64** 3045
[4] Rivas J, Hueso L E and Fondado A 2000 *J. Magn. Magn. Mate.* **22** 157
[5] Barnard J A, Fujiwara H, Inturi V R, Jarratt J D, Scharf T W and Weston J L 1996 *Appl. Phys. Lett.* **69** 2758
[6] Mawlawi D A, Coombs N and Moskovits M 1991 *J. Appl. Phys.* **70** 4421
[7] Tager A A , Xu J M and Moskovits M 1997 *Phys. Rev.* B **55** 4530
[8] Kruis F E, Nielsch K, Fissan H, Rellinghaus B and Wasserman E F 1998 *Appl. Phys. Lett.* **73** 547
[9] Shantha K, Kar S S, Subbanna G N and Raychaudhuri A K 2004 *Solid State Commun.* **129** 479
[10] Mahesh R, Mahendiran R, Raychaudhuri A K and Rao C N R 1996 *Appl. Phys. Lett.* **68** 2291
[11] Gong Z, Zhao B R, Cai C and Lin Y 2001 *Appl. Phys. Lett.* **79** 827
[12] Xu D S, Xu Y J, Chen D P, Guo G L, Gui L L and Tang Y Q 2000 *Chem. Phys. Lett.* **325** 340
[13] Sui Y C, Leon J A G, Bermudez A and Saniger J M 2001 *Carbon* **39** 1709
[14] Li P G, Fu X L, Chen L M, Zhang H Y, Li L H and Tang W H 2005 *Chin. Phys. Lett.* **22** 651
[15] Barnard J A, Fujiwara H, Inturi V R, Jarratt J D, Scharf T W and Weston J L 1996 *Appl. Phys. Lett.* **69** 2758
[16] Sun L, Ding Y, Chien C L and Searson P C 2001 *Phys. Rev.* B **64** 184430
[17] Zhao Y G, Cai W, Wu X S, Zhang X P, Wang K, Gao S N, Lu L and Zhu J 2005 *Appl. Phys.* A **81** 607
[18] Fu X L, Wang Y, Li P G, Chen L M, Zhang H Y, Tu Q Y, Li L H and Tang W H 2005 *Acta Phys. Sin.* **54** 1693 (in Chinese)
[19] Li P G, Chen C P, Fu X L, Chen L M, Zhang Y, Li L H and Tang W H 2005 *Int. Mod. Phys.* B **19** 2526
[20] Huang B X, Liu Y H, Zhang R Z, Yuan X B, Wang C J and Mei L M 2003 *J. Phys. D: Appl. Phys.* **36** 1923